







FULL PAPER

Open Access



Shallow resistivity structure around the 2018 craters of Mt. Motoshirane of Kusatsu-Shirane Volcano, Japan, revealed by audio-frequency magnetotellurics

Asami Honda^{1*} , Wataru Kanda¹ , Takao Koyama² , Shinichi Takakura³ , Yasuo Matsunaga⁴ , Tatsuji Nishizawa⁵  and Satoshi Ikezawa²

Abstract

In 2018, a phreatic eruption occurred at Mt. Motoshirane, a pyroclastic cone group of the Kusatsu-Shirane Volcano in central Japan. The eruption was abrupt, and no signs of volcanic activity have been observed in recent years, in contrast to the other major pyroclastic cone group, Mt. Shirane, which hosts the active crater lake and has endured repeated phreatic eruptions. To understand the mechanism of the eruption at Mt. Motoshirane, information on the shallow hydrothermal system, which is thought to be the source region of phreatic eruptions, is required; however, few studies have been conducted on this particular cone group. In this study, we conducted an audio-frequency magnetotelluric survey in 2020 to reveal the shallow resistivity structure around the 2018 craters. A three-dimensional resistivity structure model showed generally two layers, with high resistivities at shallow depths overlain by low resistivities underneath. The boundary between the layers corresponded to the top boundary of the Neogene basement rocks. These low resistivities were not found beneath the 2018 craters; therefore, part of the Neogene basement rocks could have been lost by the eruption beneath the 2018 craters. This is consistent with the geochemical study on the mineral assemblage of the erupted deposits, which suggested that the explosions reached the depth of the basement.

Keywords Mt. Motoshirane, Phreatic eruption, Audio-frequency magnetotellurics, Resistivity structure, Hydrothermal system

*Correspondence:

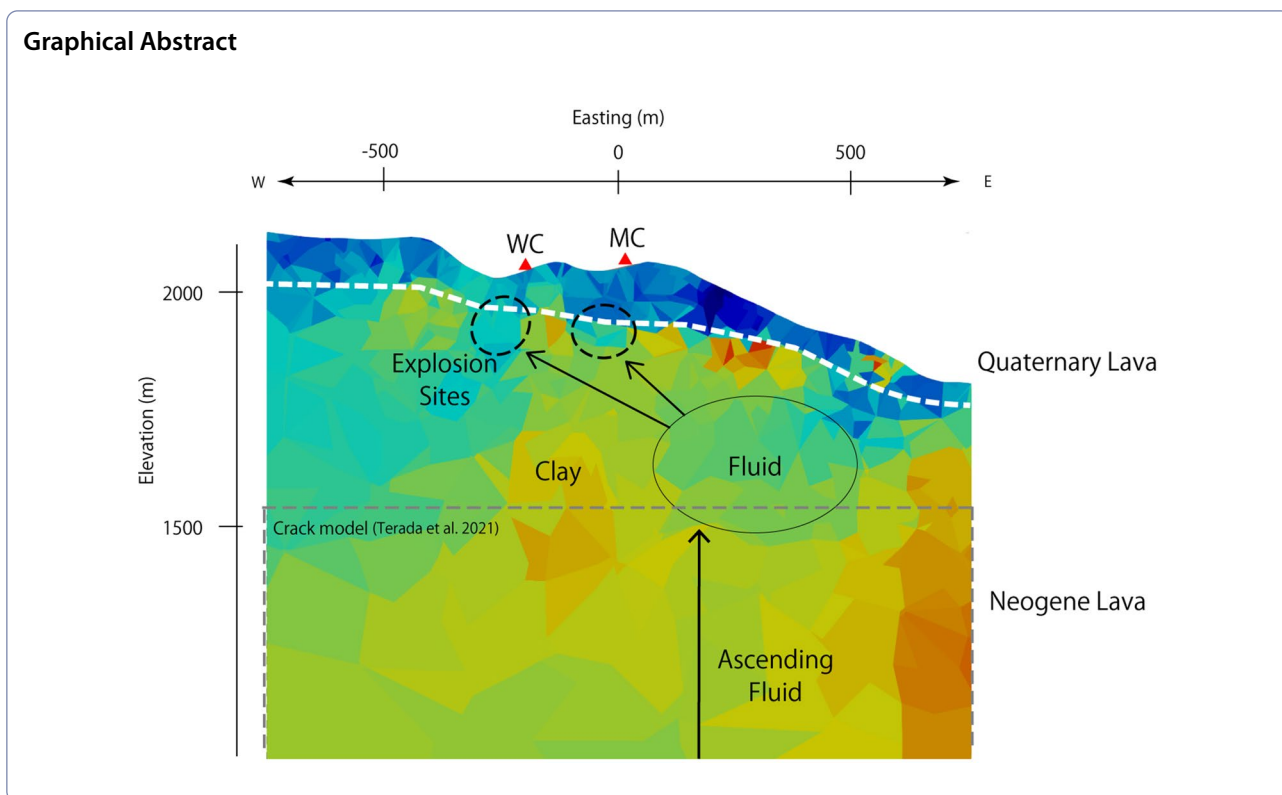
Asami Honda

honda.a.ad@m.titech.ac.jp

Full list of author information is available at the end of the article



© The Author(s) 2023. **Open Access** This article is licensed under a Creative Commons Attribution 4.0 International License, which permits use, sharing, adaptation, distribution and reproduction in any medium or format, as long as you give appropriate credit to the original author(s) and the source, provide a link to the Creative Commons licence, and indicate if changes were made. The images or other third party material in this article are included in the article's Creative Commons licence, unless indicated otherwise in a credit line to the material. If material is not included in the article's Creative Commons licence and your intended use is not permitted by statutory regulation or exceeds the permitted use, you will need to obtain permission directly from the copyright holder. To view a copy of this licence, visit <http://creativecommons.org/licenses/by/4.0/>.



Introduction

In January 2018, a phreatic eruption occurred on Mt. Motoshirane, a main pyroclastic cone group of the Kusatsu-Shirane Volcano (KSV) in central Japan (Ogawa et al. 2018). Mt. Motoshirane consists of multiple pyroclastic cones and the erupted cones are the youngest in the KSV (Ishizaki et al. 2020). Although the volume of this eruption was as low as $2.4\text{--}3.4 \times 10^4$ t (Kametani et al. 2021), the event was unexpected and sudden, and resulted in one death and eleven injuries. Analysis of the surrounding crustal deformation suggests that this eruption was caused by the ascent of fluids through subvertical cracks (Terada et al. 2021).

In the KSV, phreatic eruptions have occurred repeatedly in recent years at Mt. Shirane, another main pyroclastic cone group with an active crater lake, Yugama, which is 2 km north of Mt. Motoshirane (Fig. 1). Intensive monitoring using geophysical and geochemical methods has been conducted around the Yugama Crater Lake (YCL). For example, since the 1980s, the chemical and isotopic compositions of fumarolic gases and lake water have been repeatedly analyzed (e.g., Ohba et al. 2000, 2008). High-precision measurements have been conducted with seismometers and tiltmeters installed in three boreholes close to the YCL since 2001 for geophysical monitoring (Mori et al. 2006). In contrast, since

low volcanic activity and no surface activity around Mt. Motoshirane were observed, few studies have focused on this pyroclastic cone group, apart from several geological studies.

Phreatic eruptions often occur at shallow depths of the volcanic edifice and discharge rocks containing hydrothermally altered minerals (e.g., Browne and Lawless 2001; Ohba and Kitade 2005). Therefore, it is essential to determine the distribution of fluid and/or the altered zone in the shallow part of the volcanic edifice for a better understanding of the occurrence conditions of phreatic eruptions. Since electrical resistivity is a physical quantity that is sensitive to the presence of hydrothermal fluids and conductive clay minerals in the shallow subsurface, studies have been conducted to estimate the resistivity structure around craters where phreatic eruptions have repeatedly occurred. A characteristic structure has been clarified from the results of these studies, in which a hydrothermal reservoir that stores pressurized fluids or gases is covered with a layer of altered rocks with low permeability that functions as a cap (e.g., Pellerin et al. 1996; Seki et al. 2016, 2021; Tsukamoto et al. 2018).

Several magnetotelluric (MT) studies have been conducted to clarify the subsurface resistivity distribution of the KSV (Nurhasan et al. 2006; Matsunaga et al. 2020, 2022; Tseng et al. 2020). The underground structure

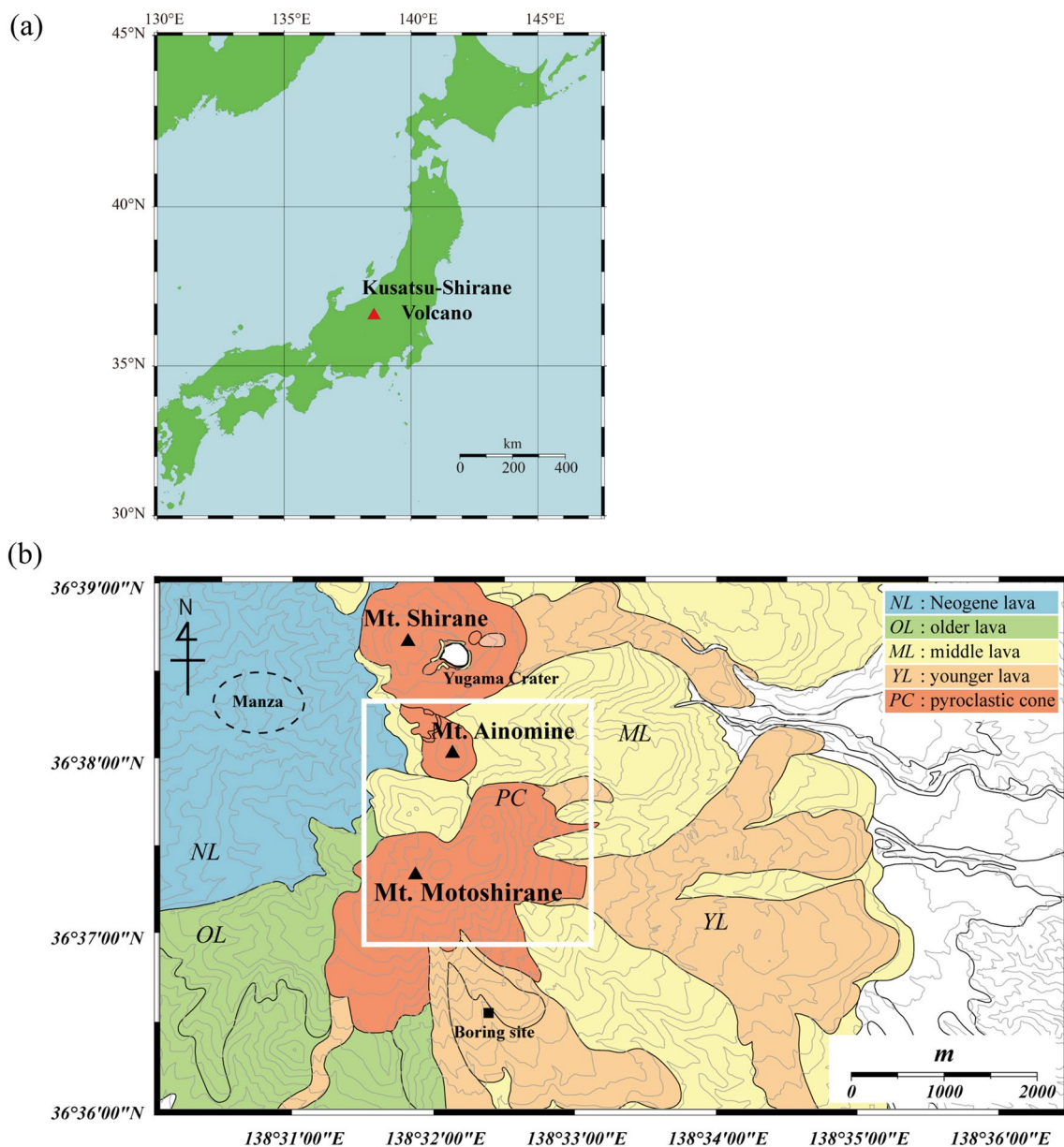


Fig. 1 **a** Location map of Kusatsu-Shirane Volcano, Japan. The red triangle represents the Kusatsu-Shirane Volcano. **b** Simplified geological map of Kusatsu-Shirane Volcano (KSV) (after Uto et al. 1983). The distribution of lava is colored by its eruptive stage. Neogene lava is the oldest. Pyroclastic cone includes volcanoclastic deposits of Motoshirane Pyroclastic Cone, Ainomine Pyroclastic Cone, and Shirane Pyroclastic Cone. Black triangles represent three pyroclastic cone groups. The white square indicates the area shown in Fig. 2. The solid square labeled Boring site indicates the location of the geothermal exploration borehole (Gunma Prefecture 1989)

around the YCL has been well investigated, and the presence of the aforementioned cap structure has also been predicted (Tseng et al. 2020). Matsunaga et al. (2020) conducted a broadband MT survey in 2015–2016 that focused on a survey line crossing Mt. Motoshirane from east to west to create a possible model of the three-dimensional (3-D) resistivity structure. Those authors found a low-resistivity region connecting Mt.

Motoshirane to Mt. Shirane at a depth of approximately 2 km and interpreted it as a reservoir that supplies fluids to the two volcanic edifices. However, because data with frequencies above 300 Hz were not used and the site spacing was coarse, the resolution for the shallow underground structure was low, and the detailed structure of the 2018 eruption site was not well-imaged. This lack of information on the shallow subsurface structure creates

uncertainty as to whether the environment around Mt. Motoshirane is prone to phreatic eruptions.

In this study, to clarify the shallow hydrothermal system of Mt. Motoshirane, we conducted an audio-frequency magnetotelluric (AMT) survey that measured high-frequency electromagnetic data to estimate the shallow subsurface structure beneath the area around the craters of the 2018 eruption. Although the AMT survey was conducted approximately two and a half years after the eruption, the eruption was so small that we assumed that the hydrothermal system was not changed significantly by the eruption, except in the vicinity of the erupted craters.

Data

The AMT survey was conducted from September 10 to 18, 2020, and the two locations where the data quality was poor were remeasured on October 27 and 28.

Measurements were made at 30 locations around the craters of the 2018 eruption (Fig. 2). The distance between the observation sites was 100–300 m around the Kagamiike-kita crater to ensure a sufficient spatial resolution. At each observation site, the MTU-5C system (Phoenix Geophysics Ltd., Toronto, Canada) was used to measure three magnetic-field components (H_x , H_y , and H_z) and two electric-field components (E_x and E_y). The magnetic field was measured using induction coils (MTC-180), and the electric field with 20–30 m long dipoles in which both ends were grounded with non-polarizing Pb-PbCl₂ electrodes. At most sites, the data were recorded for more than 12 h including nighttime, but only for 3 h during the day at certain sites to improve spatial coverage.

To improve the signal-to-noise ratio of the data, we applied the remote reference technique to each for the datasets measured simultaneously (Gamble et al. 1979; Gaubau et al. 1984) using multiple MTU-5C systems. A

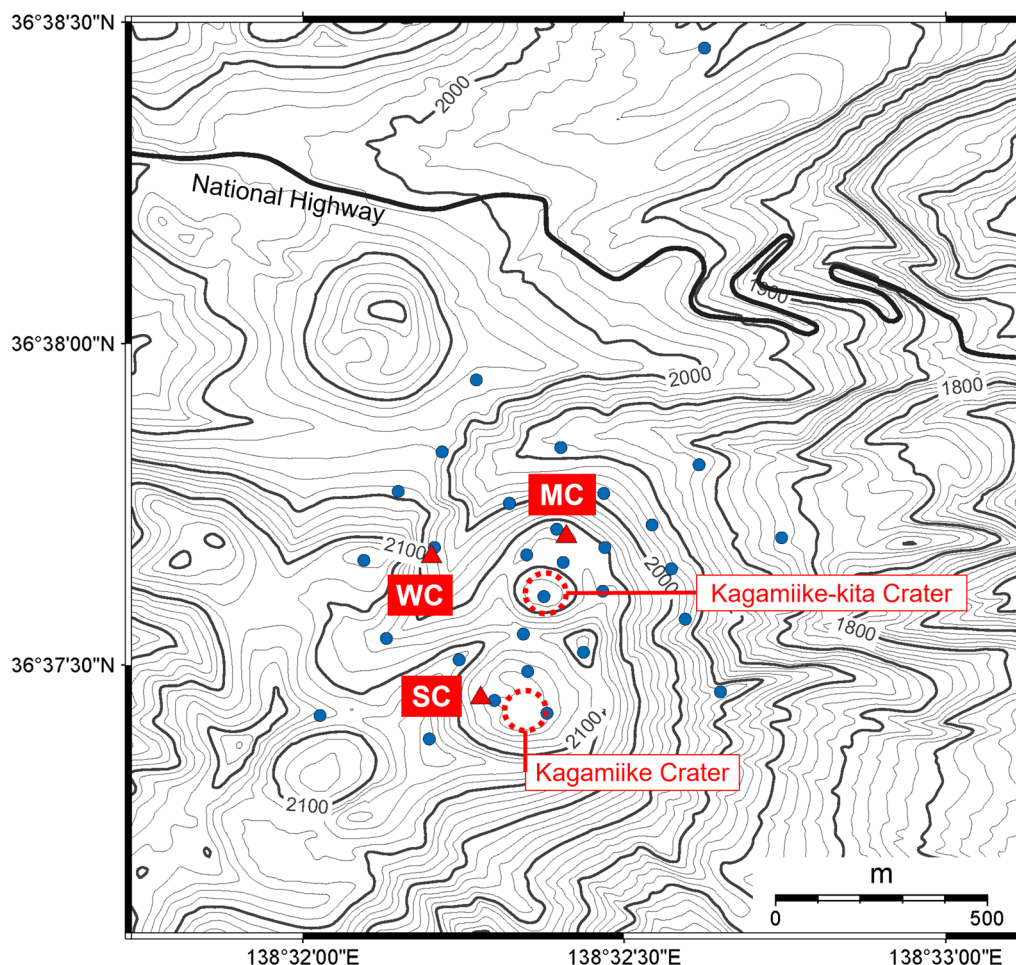


Fig. 2 Topographical map showing the survey area. Blue dots show the AMT sites. The three red triangles represent the craters of the 2018 eruption (MC = Main Crater, WC = West Crater, and SC = South Crater). Red dotted circles represent two pre-existing craters (Kagamiike-kita Crater and Kagamiike Crater) of Mt. Motoshirane. The black solid line indicates a national route

reference site was installed southeast of the YCL for the additional measurements in October. At most sites where the data were retrieved overnight, nighttime measurements from 20:00 to 05:00 were used for the analysis. The observed electromagnetic field time series data were converted to the frequency domain, and the MT responses (impedance tensor and geomagnetic transfer function) were calculated at frequencies between 10,000 and 2 Hz using Empower software (Phoenix Geophysics Ltd.).

To identify a rough trend of the horizontal resistivity distribution, the apparent resistivity distribution was calculated using one of the rotational invariants of the impedance tensor. Figure 3 shows the apparent resistivity distributions for four typical frequencies that

were calculated using the determinant of the real part of the impedance tensor \mathbf{Z} ($\det(\text{Re}\mathbf{Z})$) that is one of the rotational invariants. This quantity relatively accurately reflects the characteristics of the 3-D resistivity structure (Szarka and Menvielle 1997). As a general tendency, high resistivity is found at high frequencies and low resistivity at low frequencies, but near the surface, the resistivity values are slightly lower on the northeast side of the survey area. At frequencies below 635 Hz, an independent resistivity region is found in the vicinity of the Kagamiike-kita Crater, shown by one of the red dotted circles (Fig. 3). In addition, from the apparent resistivity distributions at 45 Hz and 5.6 Hz, it is expected that the resistivities in the deep region around

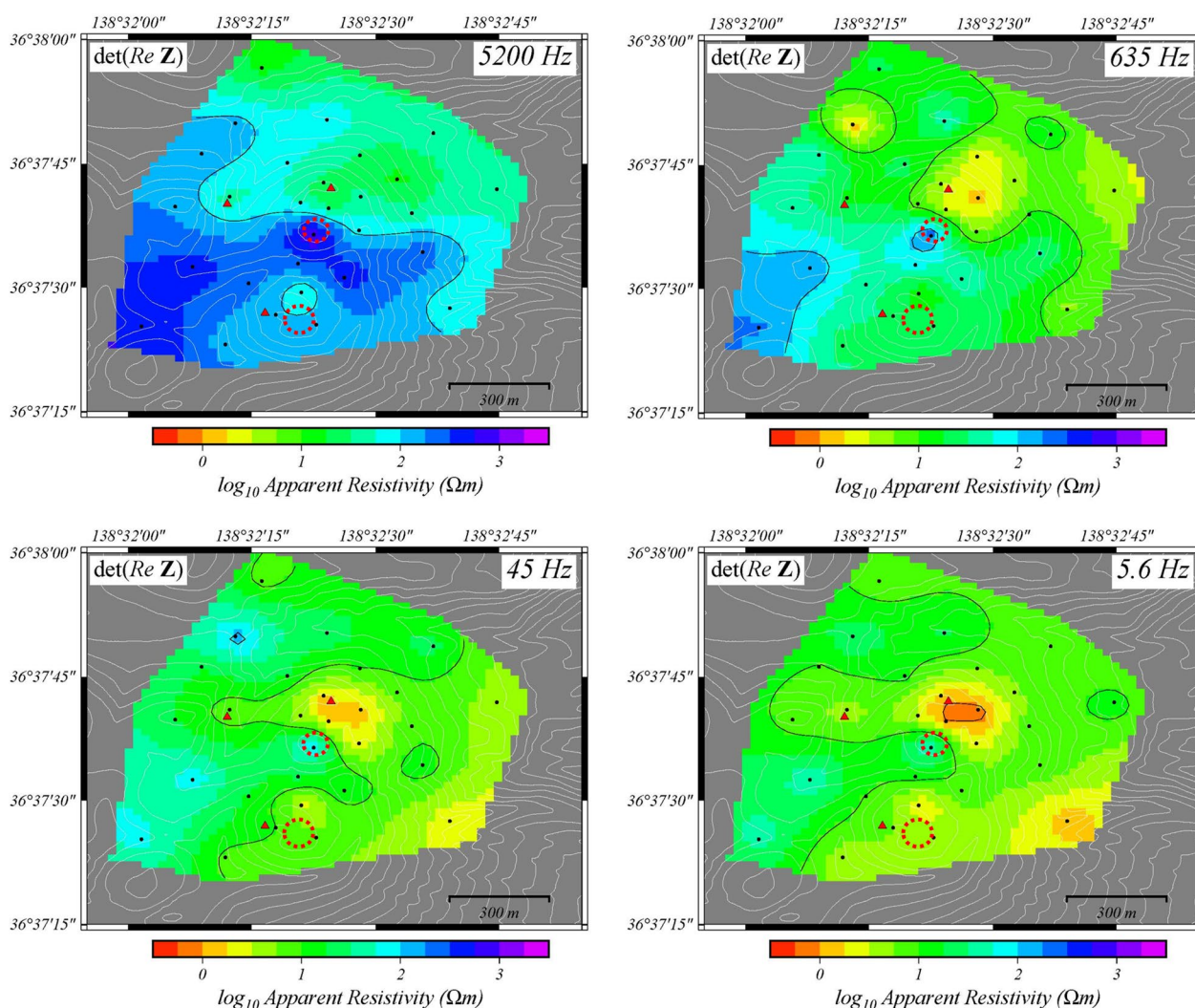


Fig. 3 Apparent resistivity distributions calculated using the rotational invariant $\det(\text{Re}\mathbf{Z})$ (the determinant of the real part of impedance \mathbf{Z}) for four representative frequencies (5200, 635, 45, and 5.6 Hz). Black dots show the AMT sites. The three red triangles represent the craters of the 2018 eruption (MC, WC, and SC in Fig. 2). Red dotted circles represent the Kagamiike-kita Crater and the Kagamiike Crater

the main crater of the 2018 eruption (MC in Fig. 2) are lower than those of the surroundings.

3-D inversion

The Kagamiike-kita and Kagamiike pyroclastic cones, which were the targets of the AMT survey, have steep topography, as shown in Fig. 2; therefore, the 3-D inversion code FEMTIC, utilizing an unstructured tetrahedral mesh that can incorporate the topographic undulation

relatively accurately (Usui 2015; Usui et al. 2017), was applied to estimate the subsurface resistivity structure. A smaller mesh size was used toward the ground surface and closer to the observation sites, while a coarser mesh was used away from the survey area. The smallest mesh size was approximately 10 m, which was used for most of the observation area. The calculation domain was 40 km (N–S) by 40 km (E–W) by 60 km (vertical), and centered on the Kagamiike-kita Crater (Fig. 4). Two types of digital elevation data were used to represent the topography. The 10-m-mesh data of the Geospatial Information Authority of Japan were used for the area within 10 km from the center of the model, and the ETOPO-1 data (Amante and Eakins 2009) were incorporated for the area further outside. Seventeen of the measured frequencies were chosen to be approximately evenly spaced on the logarithmic axis and used for the calculation. All components of the impedance tensor and geomagnetic transfer function (tipper) were used as the input data. The error floor was set at 5% for the impedance tensor and 10% for the tipper.

The following objective function was minimized for the calculation of the inversion (Usui 2015),

$$\phi(\mathbf{m}) = \phi_d(\mathbf{m}) + \alpha^2 \phi_m(\mathbf{m}_r) + \beta^2 \phi_c(\mathbf{m}_c),$$

where $\phi_d(\mathbf{m})$ is the data misfit term, $\phi_m(\mathbf{m}_r)$ is the model roughness term, $\phi_c(\mathbf{m}_c)$ is the distortion term, and α^2 and β^2 are the hyperparameters. In this study, a suitable value of α^2 was determined in the range of 0.1 to 10 under the L-curve criterion for β^2 of 0.01, 0.1, and 1 (e.g., Usui et al. 2017). For the models obtained by changing α^2 , the data misfit was plotted against the model roughness, and the model that plotted nearest to the inflection point of the L-curve was adopted as optimal (Additional file 1: Fig. S1). The L-curves obtained for different β^2 did not differ significantly, so the value of β^2 was fixed at 1.0. The initial model was set to a uniform half-space of 100 Ωm and had an RMS misfit of 9.9. After performing the inversion, the RMS misfit of the optimal model was reduced to 1.41. The responses of the optimal model, which include the estimated distortion, are shown in Additional file 1: Fig. S2a–d along with the observed data.

The horizontal sections of the optimal 3-D resistivity structure model are shown in Fig. 5. Generally, the resistivity value is high near the ground surface, and the

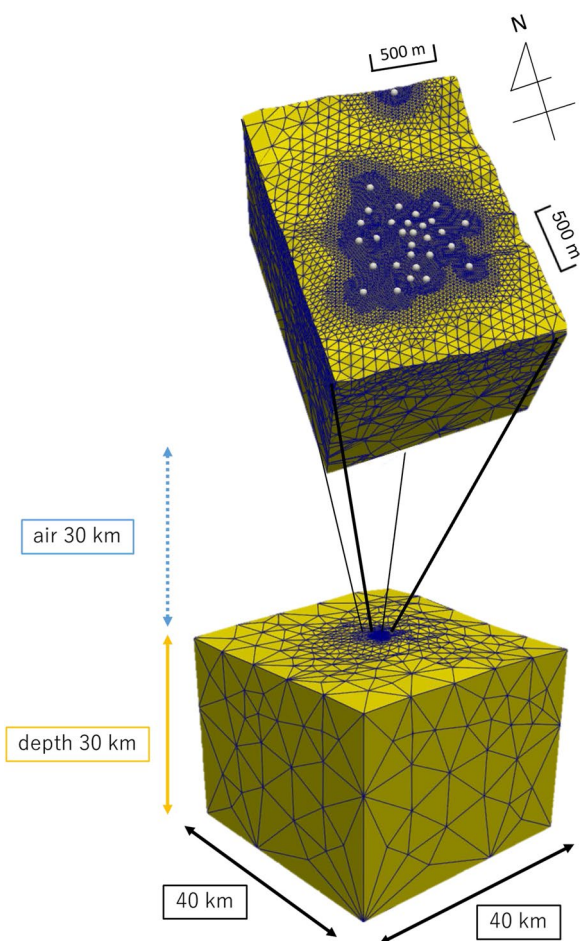


Fig. 4 Calculation domain (lower figure) and its enlargement around the survey area (upper figure). White dots represent the observation sites and navy blue lines indicate the unstructured tetrahedral mesh used in this study

(See figure on next page.)

Fig. 5 Horizontal sections of the optimal 3-D model for different five elevations (2000, 1800, 1600, 1400, and 1200 m). The topographic map is shown in the top left panel with the AMT sites (blue dots). The locations of the vertical east–west section shown in Figs. 6a, 7a, and 8 and the north–south section shown in Fig. 9 are indicated by the green and orange lines. Red triangles represent the 2018 craters (MC, WC, and SC). Gray dots in each section represent the AMT sites. The resistive feature near the surface is labeled R1, the conductive features are labeled C1 and the relatively resistive region around C1 is labeled R2. The white dashed line represents the crack model proposed by Terada et al. (2021). Black dots represent volcanic tremors just before the 2018 eruption, as suggested by Yamada et al. (2021)

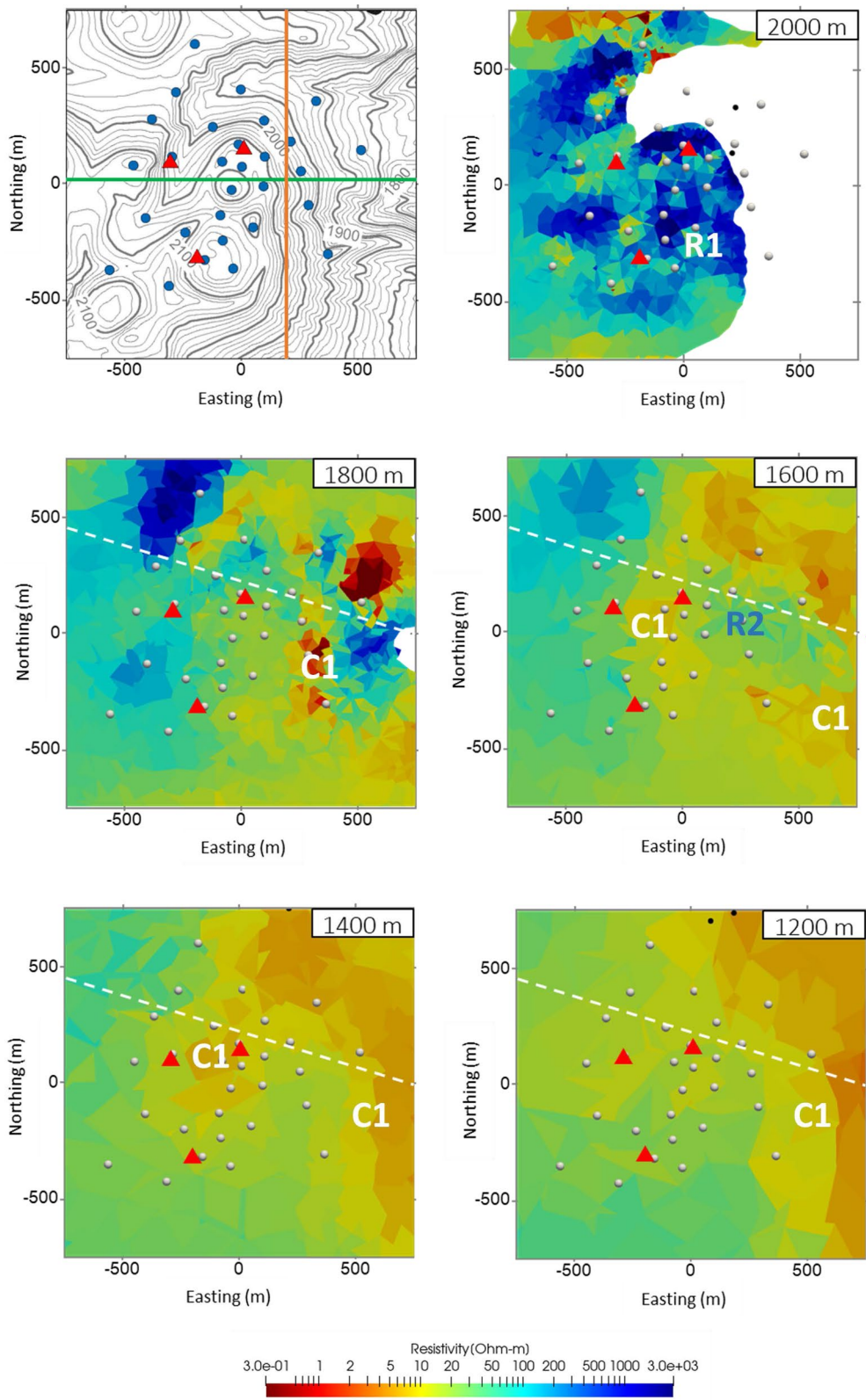


Fig. 5 (See legend on previous page.)

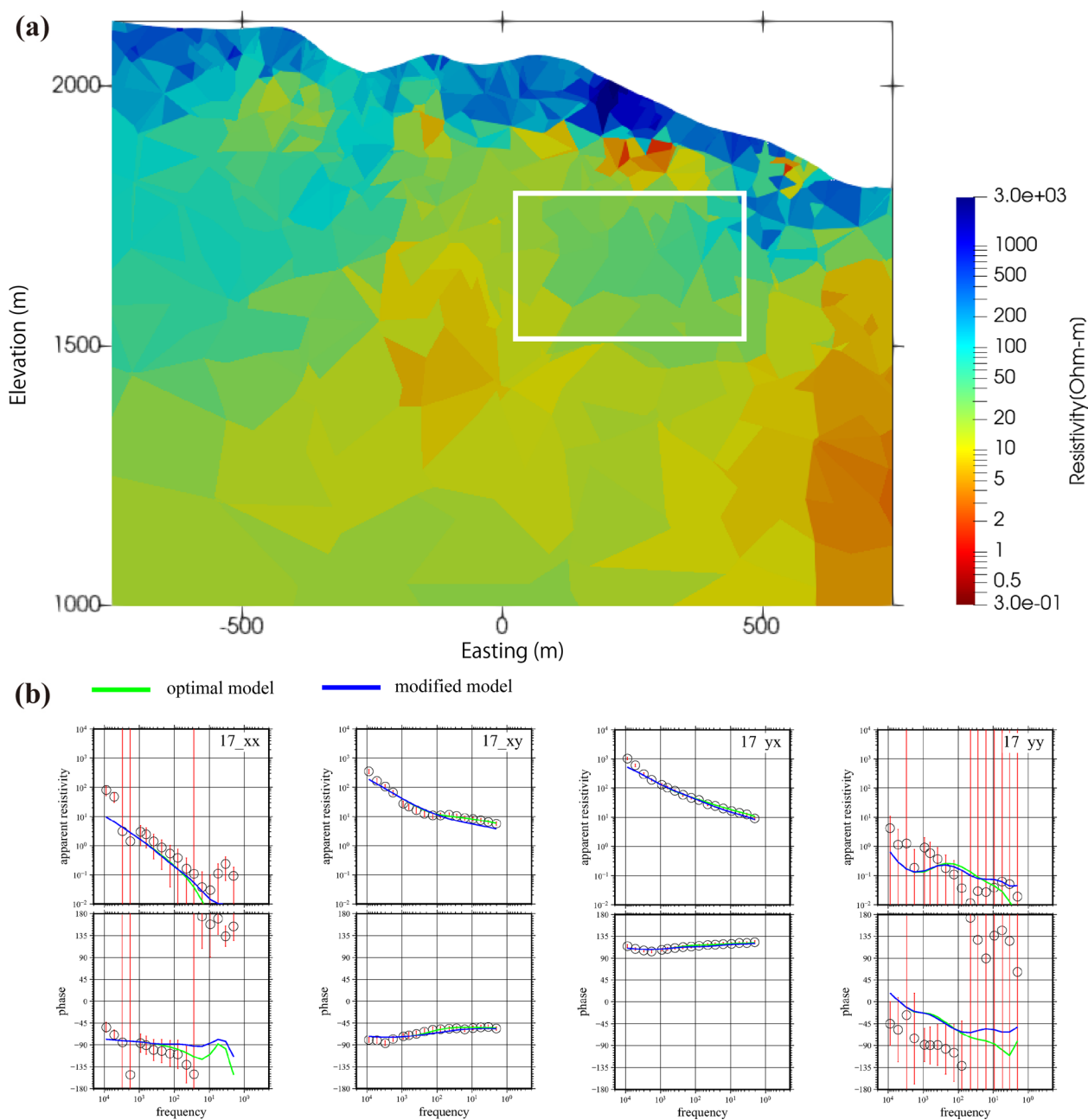


Fig. 6 Sensitivity test of the optimal 3-D resistivity structure model. **a** The east–west vertical cross-section through the Kagamiike-kita Crater of the optimal model is shown. The sensitivity of the region surrounded by the white solid line was tested. The size of the modified region was 0.5 km (N–S) by 0.6 km (E–W) by 0.4 km (vertical). **b** Sounding curves (apparent resistivity and phase) obtained from the optimal model (green), modified model (blue), and observed data (open circles with red error bars) at Site 17 directly above the modified region are shown

low-resistivity region increases with depth, which is consistent with the tendency found in the apparent resistivity distribution (Fig. 3). The low-resistivity region is not uniformly distributed, indicating that the subsurface of Mt. Motoshirane has a heterogeneous structure.

To determine how well the optimal model explained the data, we compared the model responses with the

observed data using the phase tensor (Caldwell et al. 2004) and induction arrow (Parkinson 1962) (in Additional file 1: Fig. S3). We observed a general agreement from high to low frequencies for both the phase tensor ellipses and the induction arrows, although there was some discrepancy on the northeast side at high

frequencies. The obtained model appeared to well represent the observed data.

Figure 6a shows the east–west vertical cross-section through the Kagamiike-kita Crater of the optimal 3-D resistivity model. As described above, the 50–100 m thick surface layer showed high resistivity, and the low-resistivity region extended below. In particular, a low-resistivity layer of 10 Ωm or less was present at a depth of 100–150 m on the eastern flank, and a moderately conductive region of 20–30 Ωm was found beneath it. West of this moderately low-resistivity region, low resistivities of 10 Ωm or less were distributed subvertically. Since it is difficult to constrain the structure directly beneath the conductor and the subvertical structure by the electromagnetic sounding method, we analyzed whether these regions were sensitive.

First, the sensitivity of the moderately low-resistivity region beneath the conductor was tested (Fig. 6). The resistivity of the region surrounded by the white solid line in Fig. 6a was modified to 5 Ωm , and the forward calculation of the modified model was performed to investigate changes in the sounding curves and the RMS misfit value. In Fig. 6b, the frequency responses of the apparent resistivity and phase of the site located directly above the modified region (Site 17) are shown along with the observed data. The responses of the modified model deviated from those of the optimal model at frequencies below 100 Hz, particularly in the x_y and y_y components. The RMS misfit value increased from 1.41 to 1.54. Therefore, this moderately low-resistivity region was considered to have sufficient sensitivity.

Next, the sensitivity of the subvertical conductor at altitudes of 1200–1700 m within the Kagamiike-kita pyroclastic cone was tested (Fig. 7). Similar to the previous test, the resistivities of the region surrounded by the white solid line in Fig. 7a were modified to 100 Ωm , and the sounding curves and RMS misfit value of the modified model were investigated. Comparing the sounding curves of the modified model at Site 15 with those of the optimal model, clear deviations were observed at frequencies lower than 100 Hz for all components of the apparent resistivity, and slight changes also occurred in the phase curves. Since the RMS misfit value increased to 1.66, it was determined that this subvertical conductor also had sufficient sensitivity.

Discussion

In the optimal 3-D resistivity structure model, a highly resistive layer with a thickness of ~ 100 m near the surface (R1 in Figs. 8, 9) and an underlying conductive layer (C1) were found. From the geological map of the KSV (Uto et al. 1983), the surface layer of Mt. Motoshirane is composed of Quaternary lavas and pyroclastics,

with Neogene lavas distributed beneath. These Neogene lavas are considered the basement rocks of the KSV that dip to the east, are exposed around the Manza area to the west, and are estimated to be distributed at an altitude of ~ 2000 m around Mt. Motoshirane based on the geological study (Hayakawa 1983). According to the geothermal exploration borings approximately 2.9 km south of the Kagamiike-kita Crater, these Neogene lavas are hydrothermally altered and contain smectite, a type of clay mineral (Gunma Prefecture 1989). Smectite has swelling properties and is electrically conductive with hydrologically low permeability.

The conductive region C1 is distributed at altitudes of 1800–1900 m or below (Figs. 8, 9). A low-resistivity layer with depths corresponding to C1 was widely found in the broadband MT survey around Mt. Motoshirane, and it was interpreted as altered Neogene lavas containing smectite (Matsunaga et al. 2020, 2022). Based on these, C1 is suggested to be altered Neogene lavas that correspond to the basement rocks of the KSV, and overlying R1 is interpreted as Quaternary lavas and pyroclastics. Therefore, the boundary between R1 and C1 could correspond to the boundary with the basement rocks (white dashed line in Fig. 8).

In the vertical east–west cross-section of the model (Fig. 8), the top of the C1 conductor is not continuously distributed and disappears at two locations, as shown by the black dotted circles near the 2018 craters (MC and WC). Although the optimal 3-D model did not fit the high-frequency data at some sites as described above, we have confirmed that, assuming the continuous presence of C1 even within the regions of the black dotted circles, the modified model could not further explain the data (Additional file 1: Fig. S4). The X-ray diffraction (XRD) analysis of the volcanic ash sample ejected during the 2018 eruption suggested that the ejecta were derived from basement rocks, as the constituent minerals contained pyrophyllite (Yaguchi et al. 2019). Thus, the lack of C1 beneath the 2018 craters likely indicates that part of C1 was broken by the phreatic eruption and ejected during the eruption. C1 could be replaced with high resistivities because the rocks near the surface were brecciated by the eruption and non-conductive meteoric water has infiltrated into the ground. Evidence for this is that the Kagamiike Crater, which is close to one of the 2018 craters, had formed a crater lake that accumulated meteoric water, but the lake lost water and has not yet returned to its previous state. An electrically conductive and low-permeability clay-rich layer (shallow C1 in this case) serves as the base for the infiltrated meteoric groundwater (e.g., Nurhsan et al. 2006; Aizawa et al. 2009; Kanda et al. 2010), thus having maintained the crater lake before

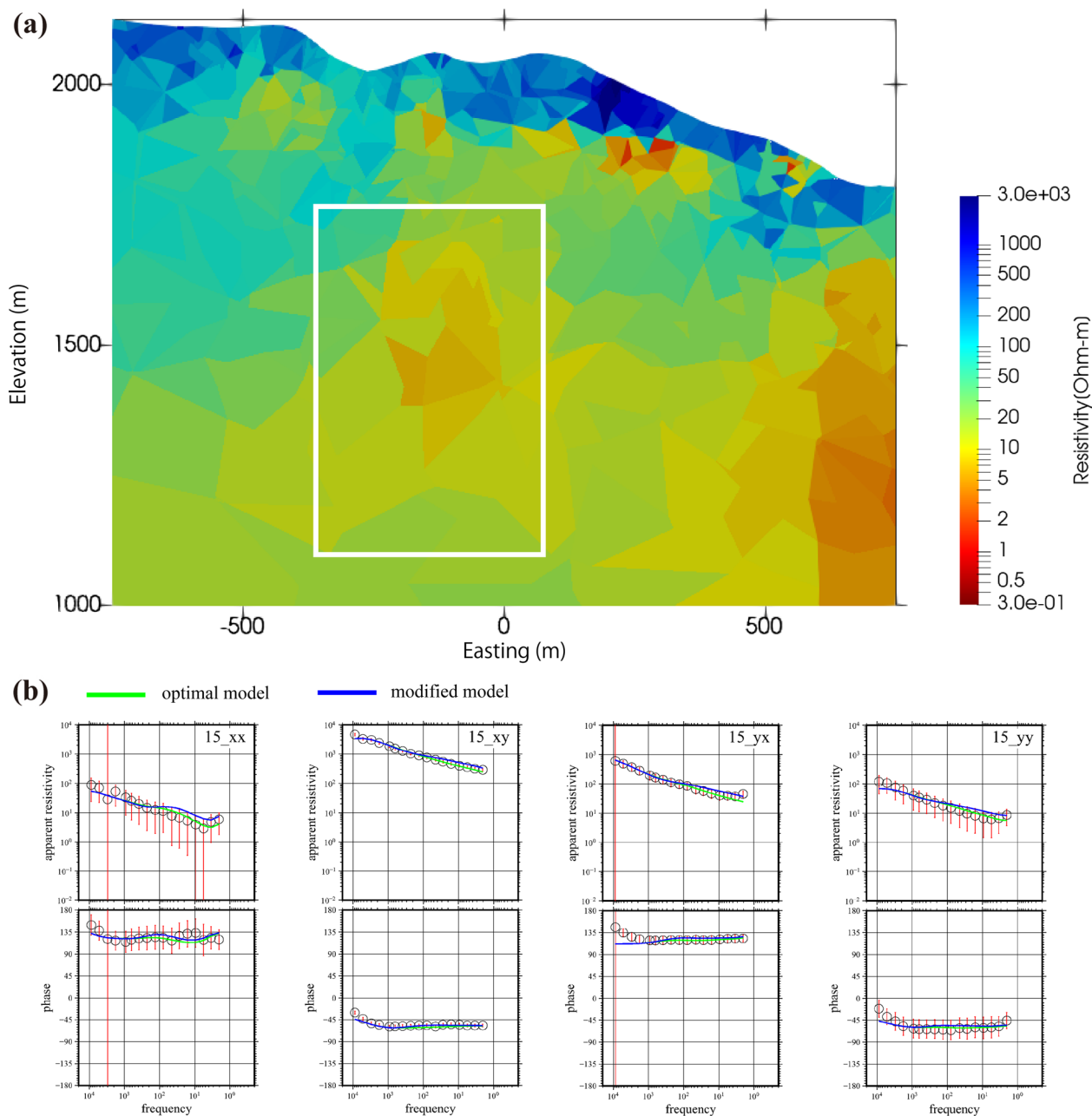


Fig. 7 Sensitivity test of the optimal 3-D resistivity structure model. **a** The east–west vertical cross-section through the Kagamiike-kita Crater of the optimal model is shown. The sensitivity of the region surrounded by the white solid line was tested. The size of the modified region was 0.6 km (N-S) by 0.5 km (E-W) by 0.6 km (vertical). **b** Sounding curves (apparent resistivity and phase) obtained from the optimal model (green), modified model (blue), and observed data (open circles with red error bars) at Site 15 directly above the modified region are shown

the eruption. Therefore, the explosions occurred in the shallow subsurface, 100–150 m from the ground surface.

In the Owakundani geothermal field of the Hakone Volcano, where a very small phreatic eruption occurred in 2015, XRD analysis of ejecta and cutting samples of a borehole suggested that the explosion occurred at a depth of 100 m or less from the surface (Mannen et al.

2019). Iwo-yama of the Kirishima Volcano also experienced a small phreatic eruption in 2018. The pressure source was estimated to be ~ 30 m from the surface based on the analysis of interferometric synthetic aperture radar (InSAR) data, and it is believed that the pressure source location is where the eruption occurred (Narita et al. 2020). Aizawa et al. (2022) recently suggested that

the explosion of Iwo-yama occurred at the zone of near-surface groundwater (80–150 m depth) beneath the erupted vent by the direct liquid-to-gas phase transition. Based on these examples, it is reasonable to assume that Mt. Motoshirane’s explosions in 2018 occurred at a depth of 100–150 m.

In Fig. 8, the region of relatively high resistivity (R2) is surrounded by the conductive regions labeled C1. Previous studies have suggested the presence of hydrothermal fluids in the shallow subsurface of Mt. Motoshirane. Yamada et al. (2021) indicated fluid migration at altitudes of 1000–1500 m based on the analysis of volcanic tremors just prior to the 2018 eruption. Himematsu et al. (2020) also interpreted the crack explaining the local deformation estimated from the analysis of InSAR data before and after the eruption as a pathway of volcanic fluids. Therefore, this region (R2) could correspond to a fluid reservoir. In this case, the altered C1 layer directly above acted as a cap layer. In Owakudani of the Hakone Volcano, a region of moderate resistivity considered a gas-rich zone was found beneath a thin low-resistivity layer, which was interpreted as a cap rock near the surface (Seki et al. 2021). A similar cap structure may be formed beneath Mt. Motoshirane, but because only a low-temperature fumarole is present around the summit area (Katabuchi

et al. 2002), the fluid reservoir is expected to be diluted with groundwater, causing a reduction in temperature.

Figure 9 shows a plot of the estimated source locations of the volcanic tremors from 3 min before to 30 s after the eruption (Yamada et al. 2021) on the north–south cross section of the resistivity structure (along the orange line in Fig. 5). Note that the discussion here assumes that the subsurface structure has not changed significantly due to the eruption, except to a depth of ~100 m in the vicinity of the erupted craters. Most tremors occur in the slightly higher resistivity region around the conductor (C1). The tremors before the eruption occurred at altitudes of 1000 to 1500 m approximately 1 km north of the erupted crater (MC), but immediately after the eruption, they moved to a shallow area around the crater. A crack model estimated from the tilt changes before and after the eruption (Terada et al. 2021) is also shown in Fig. 9. Terada et al. (2021) suggested that the opening of this crack due to the ascent of fluids from depth caused the phreatic eruption in 2018. The top of the crack reaches conductive region C1, and if such a fluid ascending path is established, it is assumed that the altered basement rock layer also contains hydrothermal fluids. This supports the idea that R2 shown in Figs. 8 and 9 (beneath the MC at altitudes of 1500–1800 m) had formed a fluid reservoir. However,

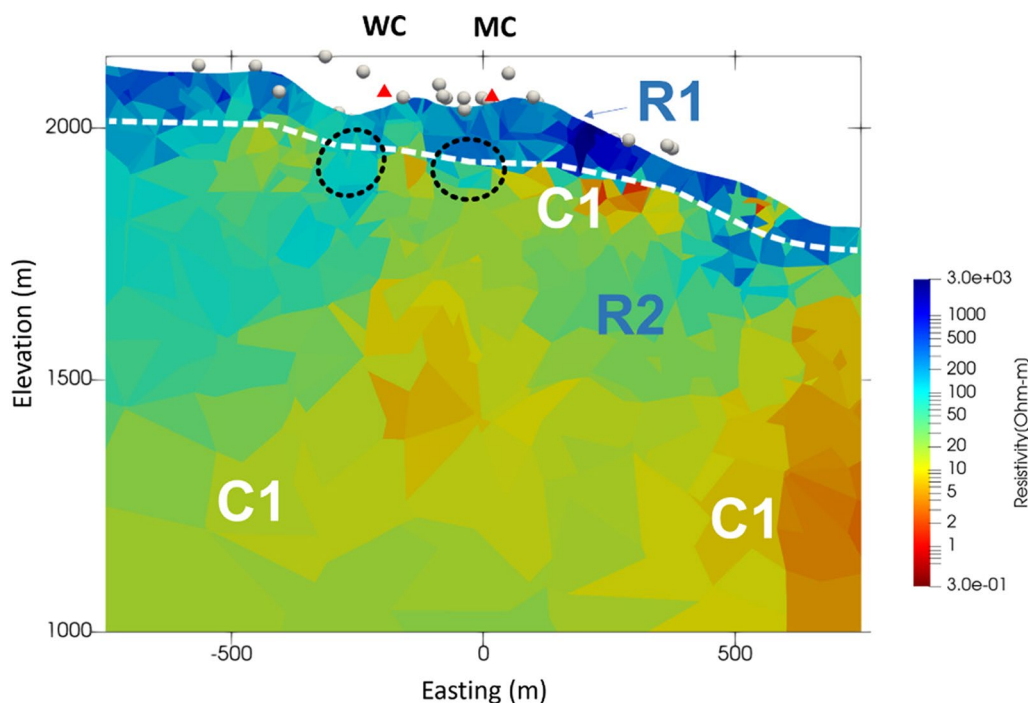


Fig. 8 East–west vertical cross-section across the Kagamiike-kita Crater of the optimal 3-D resistivity model. The red triangles represent the craters of the 2018 eruption (MC and WC). Labels indicating the resistivity features are the same as in Fig. 5. The white dashed line indicates the interpreted boundary of the basement rock. In the areas indicated by the black dotted circles, it is suggested that C1 beneath the surface resistive layer was missing due to the eruption. A possible fluid reservoir is indicated by R2

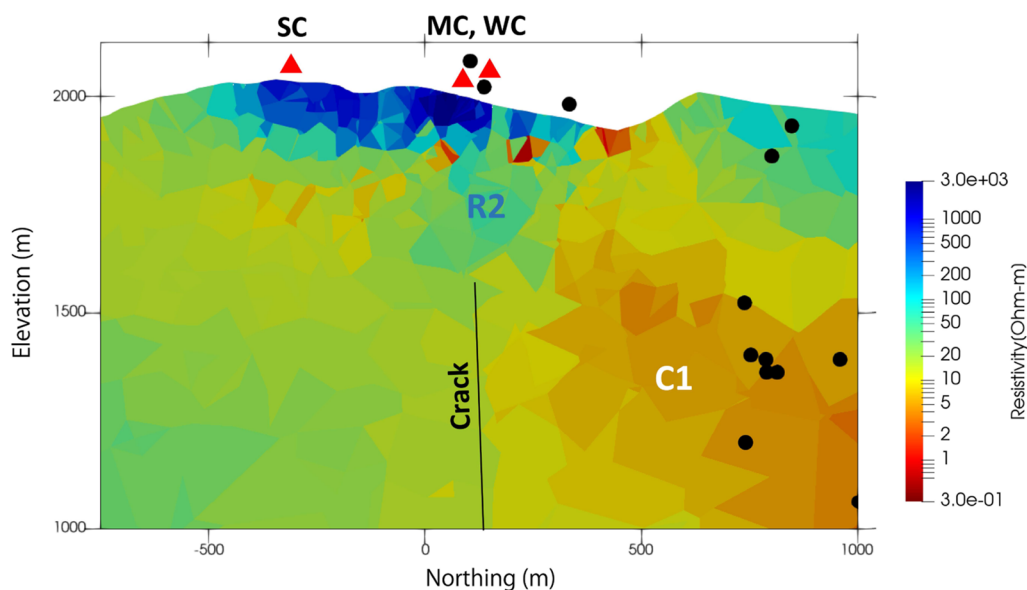


Fig. 9 Source locations of the volcanic tremors and a crack model related to the 2018 eruption shown on the north–south cross-section of the 3-D resistivity model. The red triangle represents the main crater of the 2018 eruption (MC). Black dots represent volcanic tremors just before the 2018 eruption, as suggested by Yamada et al. (2021). The black line represents the crack model indicated by Terada et al. (2021)

our model was unable to explain deeper underground. To identify deeper fluid pathways, further observations over a wider area are necessary.

A schematic of the hydrothermal system related to the 2018 eruption is shown in Fig. 10. Prior to the 2018 eruption, the shallow edifice of Mt. Motoshirane was

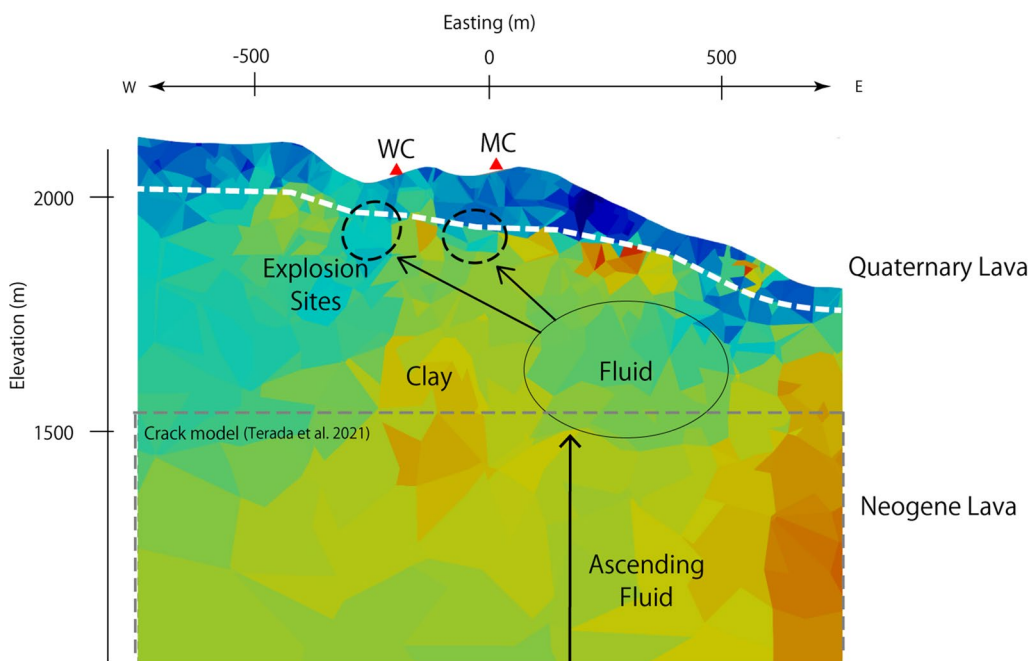


Fig. 10 Schematic model of the shallow hydrothermal system of Mt. Motoshirane related to the 2018 eruption based on the E-W cross section of the 3-D resistivity structure shown in Fig. 8. The white dashed line represents the boundary of the basement rock. Black arrows show the movement of fluids. Gray dotted line represents the crack model proposed by Terada et al. (2021). Note that the crack model is approximately parallel to this resistivity cross-section

composed of Quaternary lavas with high resistivity near the surface (R1), altered Neogene lavas with low resistivity (C1), and a fluid reservoir with moderate resistivity (R2). This fluid reservoir is likely to be at a lower temperature, but is affected by volcanic fluids to some extent. Immediately before the 2018 eruption, high-temperature hydrothermal fluids were transported to shallow levels through the pre-existing crack (Terada et al. 2021). In this shallow subsurface, there was a poorly permeable layer and the above-mentioned fluid reservoir underneath. The phreatic eruption likely occurred because of the rapid supply of hot hydrothermal fluids from depth to the reservoir, which destroyed part of the overlying altered layer. To verify this hypothesis, it is necessary to perform hydrothermal simulations based on the resistivity structure and examine the types of hydrothermal processes that occurred before the eruption.

Conclusions

We conducted an audio-frequency magnetotelluric survey in 2020 to clarify the resistivity structure of the shallow hydrothermal system of Mt. Motoshirane, which experienced a small phreatic eruption in 2018. The following results were obtained from the inferred three-dimensional resistivity structure model.

1. The subsurface structure of Mt. Motoshirane basically has a two-layer structure composed of a high-resistivity layer (R1) corresponding to the Quaternary lavas near the surface and low resistivities (C1) corresponding to the altered Neogene lavas below. The low-resistivity layer is interpreted to be the basement rock of Kusatsu-Shirane Volcano.
2. The upper part of the basement rock, which is characterized by a highly conductive zone, was not found beneath the 2018 craters. This is probably because part of the conductive basement rock was destroyed by the eruption, signifying the likely locations where the eruption occurred.
3. A moderate-resistivity region in the low-resistivity layer (R2) could be a fluid reservoir. The 2018 eruption is considered to have occurred because of the rapid supply of high-temperature volcanic fluids to this region through the pre-existing crack immediately before the eruption.

We have estimated the mechanism behind the 2018 eruption; nevertheless, there are still uncertainties regarding fluid flow within the volcano. Reproduction of the hydrothermal process before the eruption, based on the findings obtained in this study, will be an area for future research.

Abbreviations

AMT	Audio-frequency magnetotelluric
3-D	Three-dimensional
YCL	Yugama crater lake
RMS	Root-mean-square

Supplementary Information

The online version contains supplementary material available at <https://doi.org/10.1186/s40623-023-01799-3>.

Additional file 1. Fig. S1: Plot of the data misfit and the model roughness using different trade-off parameters ($\alpha^2 = 0.10, 0.20, 0.30, 0.60, 1.0, 2.0, 3.0,$ and 6.0). The labeled numbers indicate the values of α^2 . β^2 was fixed at 1.0. Using the L-curve criterion, the model with $\alpha^2 = 0.60$ was adopted as optimal. **Fig. S2:** Comparisons of the observed data with the results of the optimal 3-D model. Comparisons of the apparent resistivity and the phase of the **a** Z_{xx} component, **b** Z_{xy} component, **c** Z_{yx} component, and **d** Z_{yy} component. Red dots with error bars indicate observed data, and green lines indicate model results. **Fig. S3:** Comparisons of the observed data with the optimal model for four representative frequencies (5200, 635, 45, and 5.6 Hz). **a** Comparison by the phase tensor. Blue ellipses show the observed data, and green ellipses show the model responses. **b** Comparison by the induction arrows. Blue and green arrows represent the real component of the induction arrow calculated from the observed data and the model responses, respectively. Right blue and yellow arrows represent the imaginary component of the induction arrow calculated from the observed data and the model responses, respectively. **Fig. S4:** A test to confirm that the C1 conductor is not continuous. **a** The east-west vertical cross-section through the Kagamiike-kita Crater of the optimal model is shown. Only the resistivity blocks between 50 and 150 Ωm within the regions surrounded by the two white squares were modified to several resistivity values. The size of the modified region was 0.4 km (N-S) by 0.4 km (E-W) by 0.1 km (vertical). **b** Sounding curves (apparent resistivity and phase) obtained from the model responses (colored lines) and observed data (open circles with red error bars) at Site 15 directly above the modified region are shown. The colored lines represent the optimal model (red), the model modified to 5 Ωm (green), the model modified to 10 Ωm (blue), and the model modified to 1000 Ωm (orange). The RMS misfit values were 1.41 (red), 2.34 (green), 1.93 (blue), and 1.55 (orange).

Acknowledgements

In conducting the AMT survey, we received cooperation from the Kusatsu Town Office, Agatsuma District Forest Office, and Shinetsu Regional Environment Office. The Japan Meteorological Agency provided support for monitoring volcanic activity during observations. We thank Akihiko Terada, Yasuo Ogawa (School of Science, Tokyo Institute of Technology), and all staff at the Volcanic Fluid Research Center of the Tokyo Institute of Technology for useful advice and discussion. We also thank Taishi Yamada (Sakurajima Volcano Research Center, Kyoto University) for providing location data of the volcanic tremors associated with the 2018 eruption. Three-dimensional inversions were performed using a Tsubame 3.0 supercomputer at the Tokyo Institute of Technology. Some figures in this study were prepared using Generic Mapping Tools software (Wessel et al. 2019).

Author contributions

All authors participated in the acquisition of the data used during this study. AH analyzed the data, constructed the 3-D resistivity model, and drafted the manuscript. WK conceived the study and revised the manuscript. All authors read and approved the final manuscript.

Funding

This study was supported by the ERI JURP 2020-G-15 in Earthquake Research Institute, the University of Tokyo, and by the Ministry of Education, Culture, Sports, Science, and Technology (MEXT) of Japan, under its Integrated Program for Next Generation Volcano Research and Human Resource Development (Grant No. JPJ005391). This work was also supported by JSPS KAKENHI Grant No. JP21K03680.

Availability of data and materials

All data are presented as diagrams in Additional file 1: Figs. S2 and S3. Those data and the final resistivity structure model are available from the corresponding author on request.

Declarations**Ethics approval and consent to participate**

Not applicable.

Consent for publication

Not applicable.

Competing interests

No competing interests.

Author details

¹School of Science, Tokyo Institute of Technology, 2-12-1 Ookayama, Meguro, Tokyo 152-8551, Japan. ²Earthquake Research Institute, The University of Tokyo, 1-1-1 Yayoi, Bunkyo, Tokyo 113-0032, Japan. ³Geological Survey of Japan, National Institute of Advanced Industrial Science and Technology (AIST), 1-1-1 Higashi, Tsukuba, Ibaraki 305-8567, Japan. ⁴Tokyo Institute of Technology, 2-12-1 Ookayama, Meguro, Tokyo 152-8551, Japan. ⁵Mount Fuji Research Institute, Yamanashi Prefectural Government, 5597-1 Kenmarubi, Kamiyoshida, Fujiyoshida, Yamanashi 403-0005, Japan.

Received: 30 September 2022 Accepted: 4 March 2023

Published online: 23 March 2023

References

- Aizawa K, Ogawa Y, Ishido T (2009) Groundwater flow and hydrothermal systems within volcanic edifices: delineation by electric self-potential and magnetotellurics. *J Geophys Res Solid Earth* 114(B1):B01208. <https://doi.org/10.1029/2008JB005910>
- Aizawa K, Muramatsu D, Matsushima T, Koyama T, Uyeshima M, Nakao S (2022) Phreatic volcanic eruption preceded by observable shallow groundwater flow at Iwo-Yama, Kirishima Volcanic Complex, Japan. *Commun Earth Environ* 3:187. <https://doi.org/10.1038/s43247-022-00515-5>
- Amante C, Eakins BW (2009) ETOPO1—1 arc-minute global relief model: procedures, data sources and analysis (NOAA Technical Memorandum NESDIS NGDC-24). National Geophysical Data Center, NOAA, p 19. <https://doi.org/10.7289/V5C8276M>
- Browne PRL, Lawless JV (2001) Characteristics of hydrothermal eruptions, with examples from New Zealand and elsewhere. *Earth Sci Rev* 52(4):299–331. [https://doi.org/10.1016/S0012-8252\(00\)00030-1](https://doi.org/10.1016/S0012-8252(00)00030-1)
- Caldwell GT, Bibby HM, Brown C (2004) The magnetotelluric phase tensor. *Geophys J Int* 158(2):457–469. <https://doi.org/10.1111/j.1365-246X.2004.02281.x>
- Gamble TD, Goubau WM, Clarke J (1979) Magnetotellurics with a remote magnetic reference. *Geophysics* 44(1):53–68. <https://doi.org/10.1190/1.1440923>
- Goubau WM, Maxton PM, Koch RH, Clarke J (1984) Noise correlation lengths in remote reference magnetotellurics. *Geophysics* 49(4):433–438. <https://doi.org/10.1190/1.1441678>
- Gunma Prefecture (1989) Report on the Geothermal Survey around Kusatsu-Shirane Volcano, p 374 (in Japanese)
- Hayakawa Y (1983) Geology of Kusatsu-Shirane Volcano. *J Geol Soc Jpn* 89:511–525. <https://doi.org/10.5575/geosoc.89.511>. (in Japanese with English Abstract)
- Himematsu Y, Ozawa T, Aoki Y (2020) Coeruptive and posteruptive crustal deformation associated with the 2018 Kusatsu-Shirane phreatic eruption based on PALSAR-2 time series analysis. *Earth Planets Space* 72:116. <https://doi.org/10.1186/s40623-020-01247-6>
- Ishizaki Y, Nigorikawa A, Kametani N, Yoshimoto M, Terada A (2020) Geology and eruption history of the Motoshirane Pyroclastic Cone Group, Kusatsu-Shirane Volcano, central Japan. *J Geol Soc Jpn* 126:473–491. <https://doi.org/10.5575/geosoc.2020.0022>. (in Japanese with English Abstract)
- Kametani N, Ishizaki Y, Yoshimoto M, Maeno F, Terada A, Furukawa R, Honda R, Ishizuka Y, Komori J, Nagai M, Takarada S (2021) Total mass estimate of the January 23, 2018, phreatic eruption of Kusatsu-Shirane Volcano, central Japan. *Earth Planets Space* 73:141. <https://doi.org/10.1186/s40623-021-01468-3>
- Kanda W, Utsugi M, Tanaka Y, Hashimoto T, Fujii I, Hasenaka T, Shigeno N (2010) A heating process of Kuchi-erabu-jima volcano, Japan, as inferred from geomagnetic field variations and electrical structure. *J Volcanol Geotherm Res* 189(1–2):158–171. <https://doi.org/10.1016/j.jvolgeores.2009.11.002>
- Katabuchi Y, Ohba T, Hirabayashi J, Nogami K, Ohwada M, Mizuhashi S (2002) Fumarolic and mofette gases of Kusatsu Shirane volcano. *Chikyu Monthly*. No. 39, pp 46–51 (in Japanese)
- Mannen K, Tanada T, Jomori A, Akatsuka T, Kikugawa G, Fukazawa Y, Yamashita H, Fujimoto K (2019) Source constraints for the 2015 phreatic eruption of Hakone volcano, Japan, based on geological analysis and resistivity structure. *Earth Planets Space* 71:135. <https://doi.org/10.1186/s40623-019-1116-5>
- Matsunaga Y, Kanda W, Takakura S, Koyama T, Saito Z, Seki K, Suzuki A, Kishita T, Kinoshita Y, Ogawa Y (2020) Magmatic hydrothermal system inferred from the resistivity structure of Kusatsu-Shirane Volcano. *J Volcanol Geotherm Res* 390:106742. <https://doi.org/10.1016/j.jvolgeores.2019.106742>
- Matsunaga Y, Kanda W, Koyama T, Takakura S, Nishizawa T (2022) Large-scale magmatic-hydrothermal system of Kusatsu-Shirane Volcano, Japan, revealed by broadband magnetotellurics. *J Volcanol Geotherm Res*. 429:107600. <https://doi.org/10.1016/j.jvolgeores.2022.107600>
- Mori T, Hirabayashi J, Nogami K, Onizawa S (2006) A new seismic observation system at the Kusatsu-Shirane volcano. *Bull Volcanol Soc Jpn* 51:41–47. https://doi.org/10.18940/kazan.51.1_41. (in Japanese with English Abstract)
- Narita S, Ozawa T, Aoki Y, Shimada M, Furuya M, Takada Y, Murakami M (2020) Precursory ground deformation of the 2018 phreatic eruption on Iwo-Yama volcano, revealed by four-dimensional joint analysis of airborne and spaceborne InSAR. *Earth Planets Space* 72:145. <https://doi.org/10.1186/s40623-020-01280-5>
- Nurhasan, Ogawa Y, Ujihara N, Tank SB, Honkura Y, Onizawa S, Mori T, Makino M (2006) Two electrical conductors beneath Kusatsu-Shirane volcano, Japan, imaged by audiomagnetotellurics, and their implications for the hydrothermal system. *Earth Planets Space* 58:1053–1059. <https://doi.org/10.1186/BF03352610>
- Ogawa Y, Aoyama H, Yamamoto M, Tsutsui T, Terada A, Ohkura T, Kanda W, Koyama T, Kaneko T, Ominato T, Ishizaki Y, Yoshimoto M, Ishimine Y, Nogami K, Mori T, Kikawada Y, Kataoka K, Matsumoto T, Kamiisi I, Yamaguchi S, Ito Y, Tsunematsu K (2018) Comprehensive survey of 2018 Kusatsu-Shirane Eruption. *Proc Symp Nat Disaster Sci* 55:25–30
- Ohba T, Kitade Y (2005) Subvolcanic hydrothermal systems: Implications from hydrothermal minerals in hydrovolcanic ash. *J Volcanol Geotherm Res* 145(3–4):249–262. <https://doi.org/10.1016/j.jvolgeores.2005.02.002>
- Ohba T, Hirabayashi J, Nogami K (2000) D/H and ¹⁸O/¹⁶O ratios of water in the crater lake at Kusatsu-Shirane volcano, Japan. *J Volcanol Geotherm Res* 97:329–346. [https://doi.org/10.1016/S0377-0273\(99\)00169-9](https://doi.org/10.1016/S0377-0273(99)00169-9)
- Ohba T, Hirabayashi J, Nogami K (2008) Temporal changes in the chemistry of lake water within Yugama Crater, Kusatsu-Shirane Volcano, Japan: implications for the evolution of the magmatic hydrothermal system. *J Volcanol Geotherm Res* 178(2):131–144. <https://doi.org/10.1016/j.jvolgeores.2008.06.015>
- Parkinson WD (1962) The influence of continents and oceans on geomagnetic variations. *Geophys J Int* 6(4):441–449. <https://doi.org/10.1111/j.1365-246X.1962.tb02992.x>
- Pellerin L, Johnston JM, Hohmann GW (1996) A numerical evaluation of electromagnetic methods in geothermal exploration. *Geophysics* 61(1):121–130. <https://doi.org/10.1190/1.1443931>
- Seki K, Kanda W, Tanbo T, Ohba T, Ogawa Y, Takakura S, Nogami K, Ushioda M, Suzuki A, Saito Z, Matsunaga Y (2016) Resistivity structure and geochemistry of the Jigokudani Valley hydrothermal system, Mt. Tateyama, Japan. *J Volcanol Geotherm Res* 325:15–26. <https://doi.org/10.1016/j.jvolgeores.2016.06.010>
- Seki K, Kanda W, Mannen K, Takakura S, Koyama T, Noguchi R, Yukutake Y, Ishikawa M, Fukai M, Harada M, Abe Y (2021) Imaging the source region of the 2015 phreatic eruption at Owakudani, Hakone Volcano, Japan,

- using high-density audio-frequency magnetotellurics. *Geophys Res Lett* 48(1):e2020GL091568. <https://doi.org/10.1029/2020GL091568>
- Szarka L, Menvielle M (1997) Analysis of rotational invariants of the magnetotelluric impedance tensor. *Geophys J Int* 129:133–142. <https://doi.org/10.1111/j.1365-246X.1997.tb00942.x>
- Terada A, Kanda W, Ogawa Y, Yamada T, Yamamoto M, Ohkura T, Aoyama H, Tsutsui T, Onizawa S (2021) The 2018 phreatic eruption at Mt. Motoshirane of Kusatsu-Shirane volcano, Japan: eruption and intrusion of hydrothermal fluid observed by a borehole tiltmeter network. *Earth Planets Space* 73:157. <https://doi.org/10.1186/s40623-021-01475-4>
- Tseng KH, Ogawa Y, Nurhasan, Tank SB, Ujihara N, Honkura Y, Terada A, Usui Y, Kanda W (2020) Anatomy of active volcanic edifice at the Kusatsu-Shirane volcano, Japan, by magnetotellurics: hydrothermal implications for volcanic unrests. *Earth Planets Space* 72:161. <https://doi.org/10.1186/s40623-020-01283-2>
- Tsukamoto K, Aizawa K, Chiba K, Kanda W, Uyeshima M, Koyama T, Utsugi M, Seki K, Kishita T (2018) Three-dimensional resistivity structure of Iwoyama Volcano, Kirishima Volcanic Complex, Japan: relationship to shallow seismicity, surface uplift, and a small phreatic eruption. *Geophys Res Lett* 45(23):12821–12828. <https://doi.org/10.1029/2018GL080202>
- Usui Y (2015) 3-D inversion of magnetotelluric data using unstructured tetrahedral elements: applicability to data affected by topography. *Geophys J Int* 202:828–849. <https://doi.org/10.1093/gji/ggv186>
- Usui Y, Ogawa Y, Aizawa K, Kanda W, Hashimoto T, Koyama T, Yamaya Y, Kagiama T (2017) Three-dimensional resistivity structure of Asama Volcano revealed by data-space magnetotelluric inversion using unstructured tetrahedral elements. *Geophys J Int* 208:1359–1372. <https://doi.org/10.1093/gji/ggw459>
- Uto K, Hayakawa Y, Aramaki S, Oosaka J (1983) Geological map of Kusatsu-Shirane Volcano. geological maps of volcanoes. 3, Geological Survey of Japan (**in Japanese**)
- Wessel P, Luis JF, Uieda L, Scharroo R, Wobbe F, Smith WHF, Tian D (2019) The generic mapping tools version 6. *Geochem Geophys Geosyst* 20:5556–5564. <https://doi.org/10.1029/2019GC008515>
- Yaguchi M, Ohba T, Numanami N, Kawaguchi R (2019) Constituent mineral and water-soluble components of volcanic ash from the 2018 eruption of Mt. Motoshirane of Kusatsu-Shirane Volcano, Japan. *J Disaster Res* 14(7):991–995. <https://doi.org/10.20965/jdr.2019.p0991>
- Yamada T, Kurokawa AK, Terada A, Kanda W, Ueda H, Aoyama H, Ohkura T, Ogawa Y, Tanada T (2021) Locating hydrothermal fluid injection of the 2018 phreatic eruption at Kusatsu-Shirane volcano with volcanic tremor amplitude. *Earth Planets Space* 73(14):1–15. <https://doi.org/10.1186/s40623-020-01349-1>

Publisher's Note

Springer Nature remains neutral with regard to jurisdictional claims in published maps and institutional affiliations.